Université de Mons
Faculté Polytechnique – Service de Mécanique Rationnelle, Dynamique et Vibrations
31, Bld Dolez - B-7000 MONS (Belgique)
065/37 42 15 – georges.kouroussis@umons.ac.be

H. N. Huynh, G. Kouroussis, O. Verlinden, E. Rivière-Lorphèvre, Modal updating of a 6-axis robot for milling application, *Proceedings of the 25th International Congress on Sound and Vibration*, Hiroshima (Japan), July 8–12, 2018.

25th International Congress on Sound and Vibration
8-12 July 2018 HIROSHIMA CALLING
ICSV25

MODAL UPDATING OF A 6-AXIS ROBOT FOR MILLING APPLICATION

Hoai Nam Huynh, Georges Kouroussis and Olivier Verlinden
University of Mons-UMONS, Faculty of Engineering, Department of Theoretical Mechanics, Dynamics and Vibrations, Place du Parc, 20-Mons (BELGIUM)
email: HoaiNam.Huynh@umons.ac.be

Edouard Rivière-Lorphèvre
University of Mons-UMONS, Faculty of Engineering, Department of Machine Design and Production Engineering, Place du Parc, 20-Mons (BELGIUM)

This paper investigates the modal characteristics of a 6-axis industrial robot and exploits them in order to identify its joint stiffness and damping. Having a good knowledge of the robot dynamics can turn out to be a critical asset to achieve precise motions or complex tasks. It is especially true in robotic machining which is a trendy process where the robot structure is continuously excited by possibly large cutting forces. A research project has therefore been started to better understand the interactions between the process and the robot. Its dynamics was studied through an experimental modal analysis whose results served to update a robot multibody model in the low frequency range. It consists of eight main bodies, each of them represented by a mass and an inertia tensor at the centre of mass. Binding them together, transmission compliance is modelled by torsional springs and dampers about the axes of motion whose constants are updated on the basis of experimental results. Focussing on the first three joints, a first set of joint stiffness and damping was determined and provided satisfactory results since first natural frequencies and mode shapes involving joint compliance were in accordance. Joint stiffness and damping were ultimately adapted to improve the correlation of the simulated and experimental frequency response functions.

Keywords: modal updating, robotics, elasto-dynamic model, milling, joint stiffness and damping.

1. Introduction

Robotic machining is a manufacturing process which increasingly attracts industrials seeking a flexible alternative to the high cost of machine tools. Though robots were first designed for assembly, pick and place or painting tasks, they are progressively affected to manufacturing tasks. Nowadays, industrial robots can achieve tasks such as welding, cutting, gluing and machining, their main advantage being a larger workspace at a lower price. Compared to other manufacturing techniques, material removal process offers the shaping of high precision parts in various materials. Nevertheless, due to the lack of joint stiffness, robotic machining is currently restricted to applications demanding a low accuracy or limited cutting forces. Targeted applications mainly focus on finishing operations such as the deburring of foundry parts, the drilling of aircraft wings or more commonly the grinding, polishing and milling of large elements. Soft materials such as wood, plastic, foam can be machined with an accuracy close to machine tools whereas thin layers of hard material such as aluminium, steel or inconel can barely be removed [1].

Driven by these limitations, a project regarding robotic machining was recently started at the University of Mons (Belguim) in order to improve the accuracy of the process whilst maintaining the productivity and the stability of the process. As a matter of fact, since the first natural frequencies are typically located around 10 Hz, industrial robots are more susceptible to vibratory instabilities. In the context of this particular application, cutting forces will periodically excite the robot structure which may lead to a sharp rise of the level of vibration. Such a phenomenon is called *chatter* and can result from the existing mode coupling between the process and the structure. It is therefore crucial to study the dynamics of the robot to identify its natural frequencies and mode shapes. This aspect constitutes one of the first steps of the project which aspires to improve the understanding of the process by developing a numerical model of robotic milling. The latter must involve the computation of the cutting forces, the update of the machined surface, the joint compliance, the link flexibility [2] and the modelling of the actuators and controllers [3].

Experimental modal analysis remains a safe bet to determine the natural frequencies of a robot and its associated mode shapes. This approach was indeed experienced by several authors leading to good correlations between experimental and simulation results. In [4], the dynamic behaviour of the ABB IRB 6660 robot is studied by exciting the robot through hammer strokes. Since the robot is a 6-axis robot equipped with a parallel arm to raise its stiffness, the identified natural frequencies started to appear around 20 Hz (without any payload). The dynamic characterisation was eventually achieved in different configurations leading to maps representing the evolution of its natural frequencies within the workspace. The dynamic behaviour of another ABB robot with the same architecture (IRB 1400) and the same experimental method was investigated by Karagulle et al. [5] who also found the first natural frequencies around 20 Hz. The shapes of the modes indicated that the joints at the base of the robot were the first to twist. When it comes to deal with 6-axis serial robots, various experimental methods were tested in the literature since they are more common in industry. Continuing with hammer tests, Bauer et al. [6] performed an experimental modal analysis of Kuka KR 210 robot conducting to the inventory of its first modes starting around 10 Hz. Within the low frequency range (0-50 Hz), the first modes involved the twisting of the first three joint axes. On the other hand, Neubauer et al. [7] proposed to excite the robot by using periodic multisine signals in the motor torques and to update its robot model with the identified stiffness and damping for the first three joints. Very good correlations were obtained by comparing measured and simulated frequency response functions (FRFs) between the input torques and the motor positions. Dumas et al. [8] developed a methodology to identify the joint stiffness by applying static loads at the end effector and measuring the resulting displacement with an external device.

Taking the first step in the experimental modal analysis of a robot, this paper presents the identification of the joint stiffness and damping of the TX200 Stäubli robot for its first three axes and one particular configuration. Elastic effects of the last three joints (spherical wrist) are of minor importance to position the end effector and are thus neglected in the study. The next section describes how the dynamic signature of the robot was determined through an experimental modal analysis using hammer strokes. A numerical model is then developed and updated by minimizing the difference between the measured and simulated natural frequencies and associated damping ratios. Joint stiffness and damping values are consequently identified and inserted in the numerical model in order to compare the mode shapes. A ultimate fitting with the measured FRFs is finally achieved before concluding.

2. Experimental modal analysis

The studied TX200 Stäubli robot was made accessible through a partnership with the *CNC solutions - VDS* company specialised in the design of special machines such as robotic machining cell. As the company is dependent upon its customer requests, the end effector of the robot was equipped with a gripper instead of a spindle at the time of performing the modal analysis. Naturally, the reduced

payload of 5 kg affected the robot eigenfrequencies. The technical data indicate that the serial robot weights one ton and offers a nominal payload of 1000 N and a repeatability of $\pm$ 0.06 mm. The robot was mounted on a pedestal of 600 mm which situated its elbow at a height of approximately 2 m in the studied configuration (Figure 1). The latter was chosen so that the robot was positioned in a milling pose in order to identify frequency modes that could hinder the machining process. If robot joints are denominated q_i with i ranging from 1 to 6, axis angles are gathered in Table 1.

Table 1: Robot axis configuration

q_1	q_2	q_3	q_4	q_5	q_6
-90.0°	28.47°	127.53°	0.0°	-66.06°	0.0°

An experimental modal analysis was carried out for the purpose of identifying the natural frequencies of the robot in the low frequency range. The robot structure was assumed linear for the exploitation of the results. It is important to note that the robot sustained its configuration thanks to its controller rather than its brakes. As a result, structural modes can be excited as it is the case during a milling operation. Hammer strokes were given onto 84 points spread over the surfaces of the robotic structure. Each impact was always made perpendicular to the surface to sufficiently excite the robot. One piezoelectric triaxial accelerometer (Dytran 3093B1) was glued on the top horizontal surface of the wrist. The roving hammer technique was afterwards applied to the whole structure while recording the level of the input force. The data acquisition system SCADAS III was used and the instrumented hammer was adorned with a soft nozzle to excite the low frequencies. The FRF of each impact point derived from the average of four measurements and the signals were then processed with the Test.Lab software 8B release. The selected frequency bandwidth ranged from 0 to 80 Hz with a frequency resolution Δf of 0.625 Hz. An exponential window with a decay of 32.9 % was used to lessen the effects of leakage on the measurements and a force window of 0.16 s was applied on the input. Measurement quality was also tracked during the process thanks to the coherence indicator. A total of 252 FRFs were retrieved and are overlapped in Figure 2 highlighting the possible first three modes.

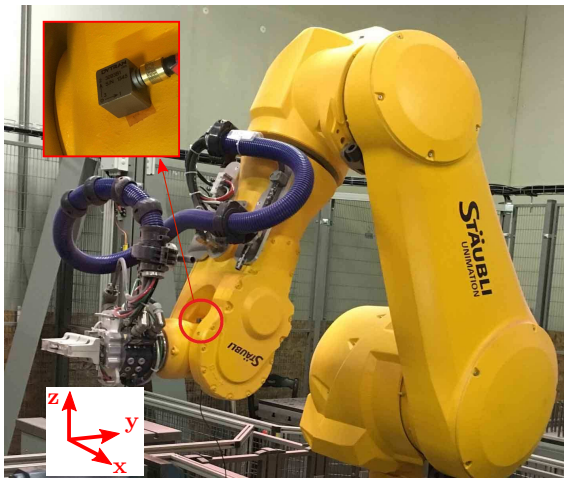

Figure 1: TX200 Stäubli robot

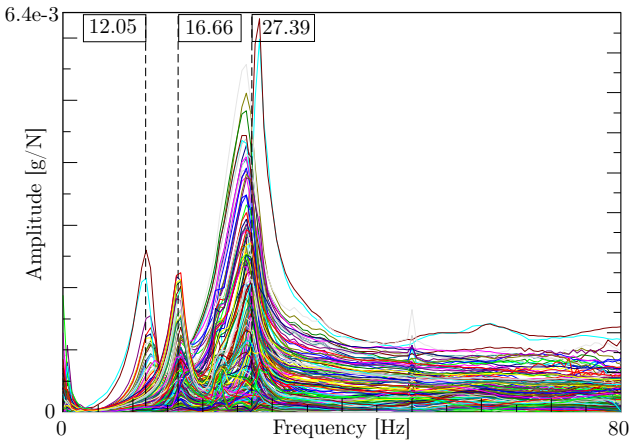

Figure 2: Overlapping of all FRFs

The analysis of the experimental results is achieved by using the Betti-Maxwell reciprocity theorem

$$H_{ij}(\omega) = H_{ji}(\omega), \tag{1}$$

switching excitation points j and response points i, as if the robot was only excited at the wrist and accelerations measured at the 84 points in the 3 directions. Each set of 84 FRFs was analysed

separately for each direction with the least-square complex exponential (LSCE) method [9] for a clear understanding of each mode influence:

- x-axis ($\perp$ to the robot plane): whereas Figure 2 showcased three main peaks, the overlap of all FRFs along the x-axis brought to light another small peak around 22 Hz only visible in that direction. Since the LSCE method could barely stabilise the pole corresponding to that frequency peak, it was believed that it was local mode that could correspond to a tilting of axis 1 around the y-axis. The mode was left aside from the study as it could not be captured with the envisaged robot model;
- y-axis (horizontal in robot plane): the analysis along the y-axis revealed two frequency peaks around 16 and 27 Hz whose poles were sufficiently stable according to the LCSE method;
- z-axis (vertical axis): the last examined direction highlighted the same peaks around 16 and 27 Hz.

Hence, the three frequency peaks at 12.05 Hz, 16.66 Hz and 27.39 Hz were considered to represent the first three main modes of the robot structure. Corresponding damping ratios were 12.3 %, 4 % and 3.55 %. As the Test.Lab software offered the possibility to animate the corresponding modes, the associated mode shapes could be observed and resulted in a rotation around axis 1 for the first mode and dominant rotations around axes 2 and 3 for the last two peaks.

3. Modelling of the 6-axis robot

A numerical model of the TX200 Stäubli robot was developed using a multibody approach. It was composed of eight rigid bodies being the base (1), the shoulder housing (2), the arm (3), the proximal forearm (4), the distal forearm (5), the wrist housing (6), the flange (7) and the gripper (8). Each body was characterised by its centre of mass position, its a mass m_i and its central tensor of inertia I_i. Inertial data were collected from CAD supplied by the robot manufacturer and redesigned afterwards to resemble as closely as possible to the real parts. The inclusion of the joint flexibility was introduced through torsional springs (with a stiffness k_i in Nm/rad) and dampers (with a damping c_i in Nms/rad) mounted in parallel along each revolution axis (Figure 3).

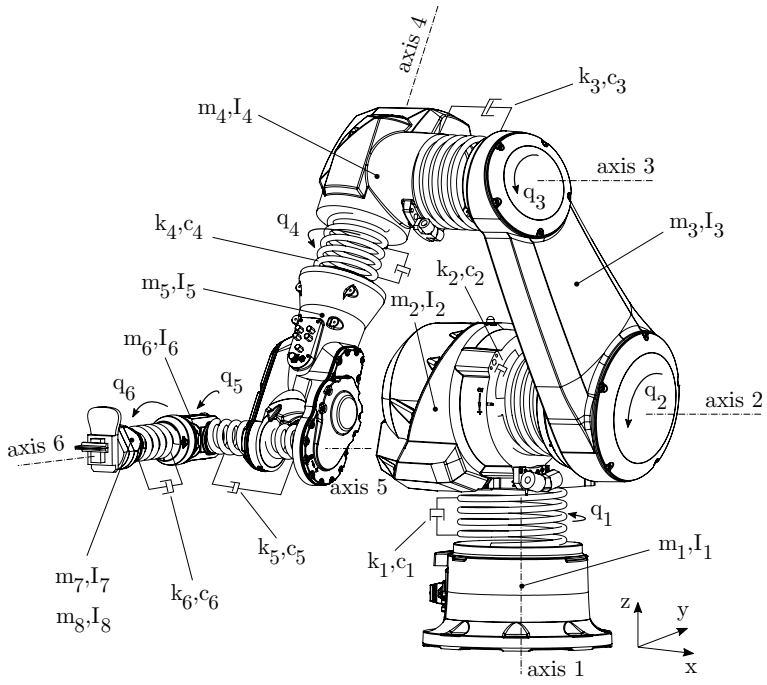

Figure 3: Robot model

From a practical point of view, the implementation of such a model was carried out using a in-house C++ multibody framework called EasyDyn allowing the dynamic simulation of mechanical systems [10]. The approach currently implemented relies on the minimal coordinates for the choice

of the configuration parameters $\mathbf{q}$ defining the motion of the bodies. The kinematics of all bodies is provided through homogeneous transformation matrices function of the chosen configuration parameters. Forces can also be applied on each body.

4. Update of the numerical model

Since the purpose of the paper is to identify the stiffness and damping of the first three joints corresponding to the experimental frequencies $f_{1-3,exp}$ and damping ratios $\xi_{1-3,exp}$, a minimisation procedure was settled using the Nelder-Mead method to find the minimum of the objective function $f(\mathbf{q}_i)$ representing the robot model.

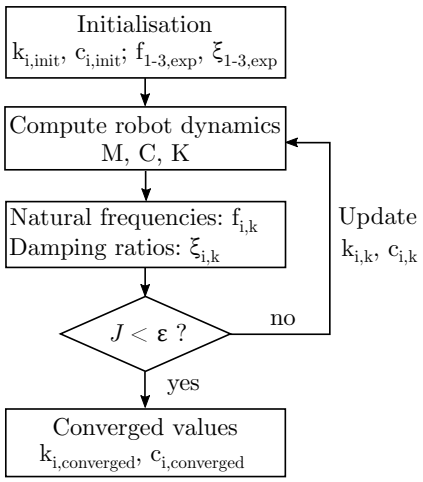

Figure 4: Iterative search of k_i and c_i

Starting with an initial guess of the stiffness $k_{i,init}$ and damping $c_{i,init}$ for all six joints, the algorithm presented in Figure 4 transmits it to the `EasyDyn` framework to compute the equations of motion of the robot model. Having built its mass and stiffness matrices, numerical eigenvalues and eigenvectors can be computed and natural frequencies $f_{i,k}$ and damping ratios $\xi_{i,k}$ are deduced. The latter are compared to their experimental counterparts and an error is computed by means of the cost function J Eq.(2) (damping ratios in %). An additional condition is formulated for the fourth natural frequencies of the simulated robot since no mode was detected between 30 and 80 Hz.

$$\begin{cases} J = & | f_{1,k} - f_{1,exp.} | + | f_{2,k} - f_{2,exp.} | + | f_{3,k} - f_{3,exp.} | + \dots \\ & | \xi_{1,k} - \xi_{1,exp.} | + | \xi_{2,k} - \xi_{2,exp.} | + | \xi_{3,k} - \xi_{3,exp.} | \\ & \text{and such as } | f_{4,k} | \geq 100 \text{ Hz} \end{cases} \tag{2}$$

If the value of the cost function J exceeds the tolerance ϵ set to 10^{-3}, the algorithm updates the stiffness $k_{i,k}$ and damping $c_{i,k}$ values for the next iteration. Once the convergence is reached, a set of stiffness $k_{i,converged}$ and damping $c_{i,converged}$ for all six joints is found ensuring a robot model excited at the experimental frequencies. Results of such a minimisation are displayed in Figure 5 in which simulated and experimental FRFs are compared. In order to obtain the simulated FRFs, the robot model was excited with a virtual hammer stroke where the sensor was located in reality. Acceleration values were recorded at the same point and the experience was repeated along the three directions. Globally, simulated frequency peaks fell at the same locations than the experimental ones excepted for the x-axis.

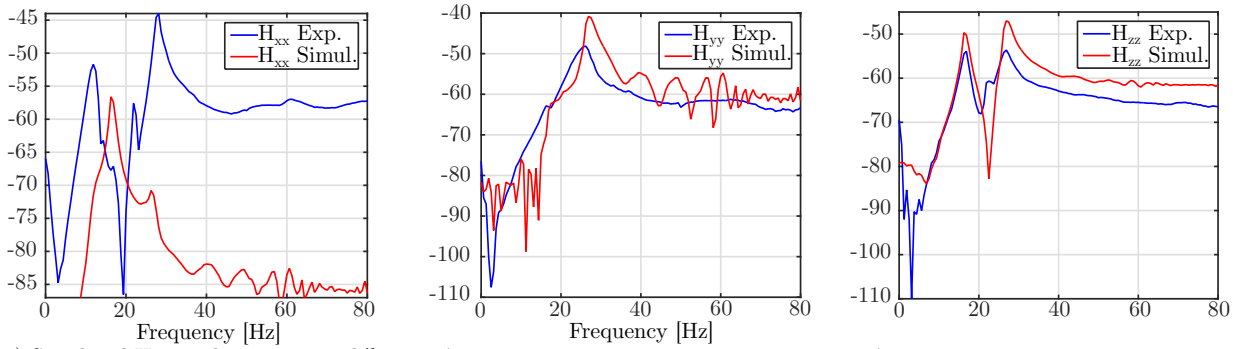

a) Simulated H_{xx} with experimental ξ b) Simulated H_{yy} with experimental ξ c) Simulated H_{zz} with experimental ξ

Figure 5: Comparison of FRFs using the experimental damping ratios

Observing that the fitting along the x and z axes could be enhanced by manually modifying the desired damping ratios, the values of the experimental damping ratios were rebalanced as follows: ξ_1=6.5 %, ξ_2=7.2 %, ξ_3=8 %. Without altering the experimental eigenfrequencies, the minimisation procedure was recovered with the new damping ratios. Once completed, the algorithm returned the converged values regarding the joint stiffness and damping of the robot (Table 2).

Table 2: Identified joint stiffness and damping

	k_i [Nm/rad]	c_i [Nms/rad]
Joint 1	$1.358 \cdot 10^6$	2371.92
Joint 2	$2.175 \cdot 10^6$	2918.17
Joint 3	$0.722 \cdot 10^6$	670.37
Joint 4	$1.559 \cdot 10^6$	316.03
Joint 5	$0.377 \cdot 10^6$	77.51
Joint 6	$1.560 \cdot 10^6$	5.89

As announced in the literature, the order of magnitude of the joint stiffness was around 10^6 Nm/rad. Among the first three joints, it seems that the second axis is the stiffer for that particular robot configuration, as it supports the majority of the robot arm. Identified joint stiffness for the last three joints must be examined cautiously as only three natural frequencies were observed experimentally. Damping values are quite high for the first three joints but progressively decrease for the upper joints.

As before, FRFs at the sensor location are compared in Figure 6. It can now be noticed that FRFs along the z-axis are well correlated in amplitude and in frequency. FRFs along the y-axis matches their frequency peaks but are a bit offset in amplitude. The worst results are obtained along the x-axis as the simulated FRF can only capture the first frequency peak at 12.05 Hz. A small peak appears at 16.66 Hz instead of 27.39 Hz.

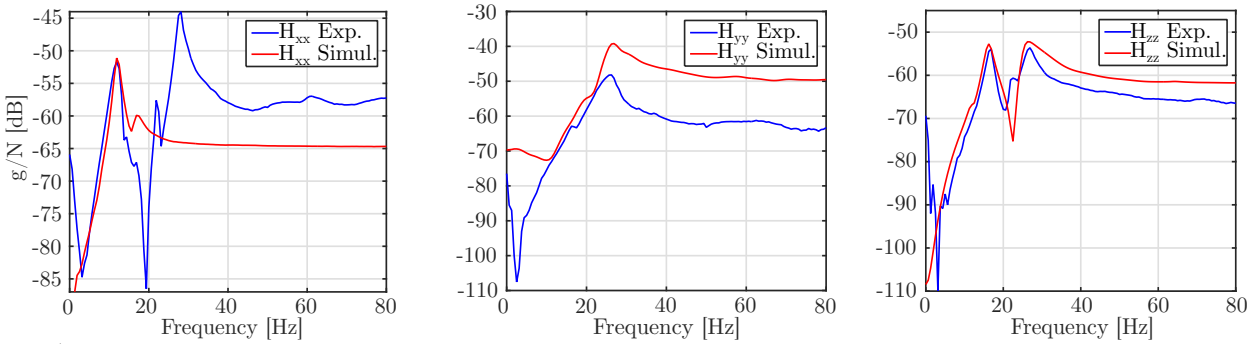

a) Simulated H_{xx} with rebalanced ξ b) Simulated H_{yy} with rebalanced ξ c) Simulated H_{zz} with rebalanced ξ

Figure 6: Comparison of FRFs using the rebalanced damping ratios

`EasyDyn` allows viewing the mode shapes of the simulated robot. Table 3 provides a descriptive summary of all mode shapes and confirms that the identified joint stiffness and damping returns the desired natural frequencies and damping ratios. As requested, the fourth natural frequency is indeed above 100 Hz.

Table 3: Identified mode shapes

Mode	Frequencies [Hz]	Damping ratios [%]	Description
Mode 1	12.05	6.5	Rotation around axis 1
Mode 2	16.66	7.2	Rotation around axis 2 and small rotation of axis 1
Mode 3	27.39	8	Rotation around axis 3
Mode 4	151.9	10.1	Rotation around axis 5 and small rotation of axes 2 and 3
Mode 5	238.1	15.4	Rotation around axis 4
Mode 6	5593	6.65	Rotation around axis 6

Focussing back on the mode shapes of the first three joints, Figure 7 depicts a comparison of the experimental and simulated mode shapes. A very good correlation is noticed:

- mode 1: the first mode is characterised by a sole motion of the first axis. Both visualisations showcased a rotation of the first axis.
- mode 2: the second mode is mainly animated by a rotation about the second axis. Although it is much harder to witness the deformation of the experimental mode shape, the extremities of the robot arm do move as if the second axis twisted. The middle of the arm seems immobile as those points where excited perpendicularly to the plan view;
- mode 3: the last examined mode exhibits a rotation about the third axis that can be visualised in both representations.

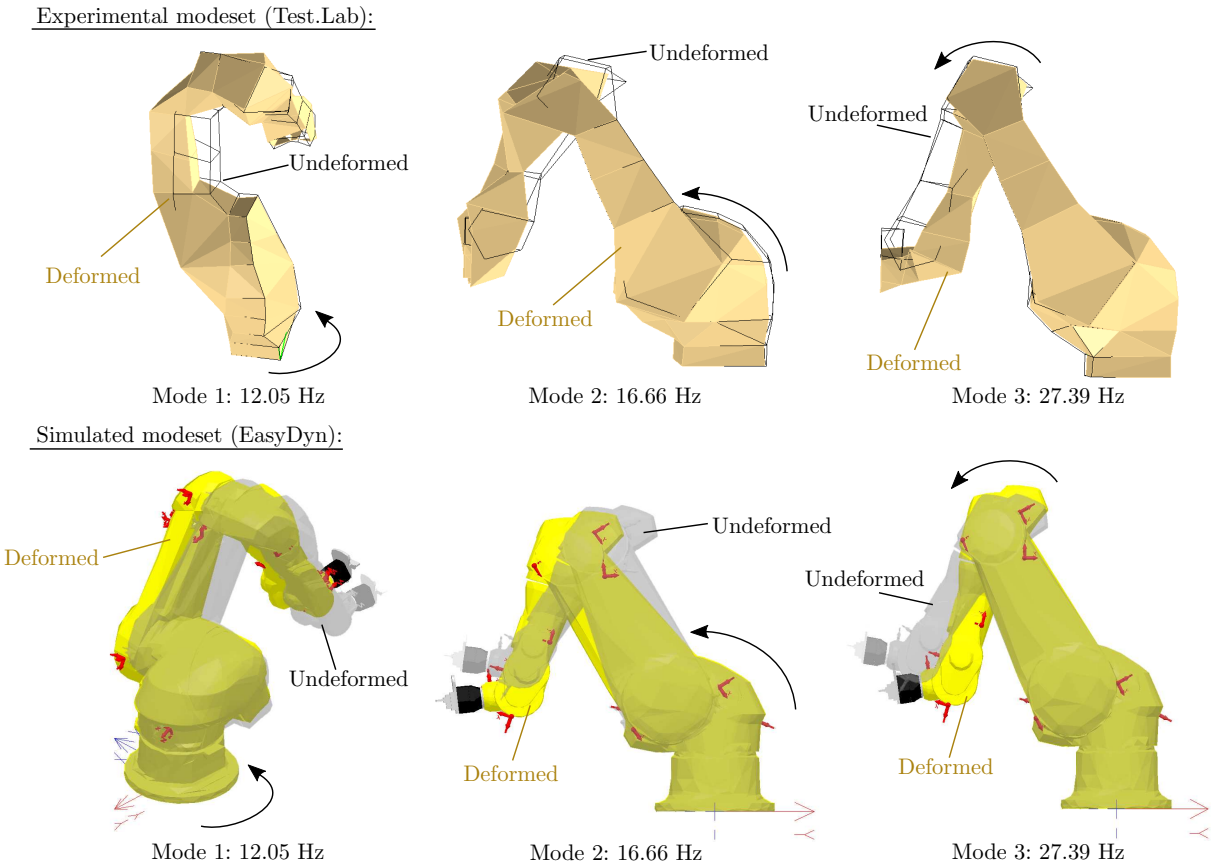

Figure 7: Comparison of the mode shapes

A last validation was made by checking the orthogonality of the simulated $\underline{\psi}_i^s$ and experimental $\underline{\psi}_i^e$ eigenvectors by using the modal assurance criterion (MAC) using the `EasyMod` toolbox [11].

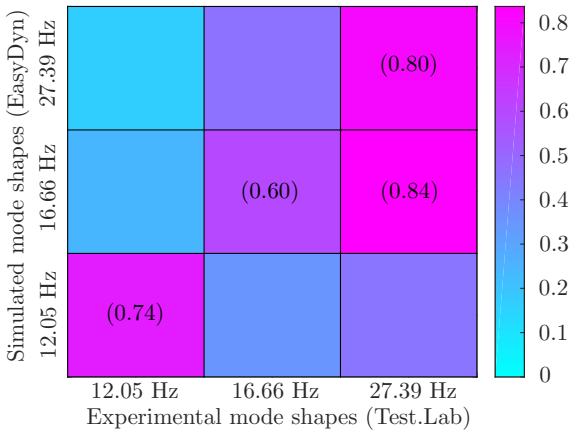

Figure 8: MAC matrix computed from Eq.(3)

$$MAC_{ij} = \frac{\left(\left\{ \underline{\psi}_i^s \right\}^T \left\{ \underline{\psi}_j^e \right\}^* \right)^2}{\| \underline{\psi}_i^s \|^2 \| \underline{\psi}_j^e \|^2} \tag{3}$$

Simulated eigenvectors were constructed by exciting the robot model at its resonance frequencies. Maximum displacements of nodes highlighted in Figure 7 were then saved. Regarding the generated MAC matrix (Figure 8), modes 1 and 3 are very well correlated whereas simulated mode 2 seems to be mistaken with experimental mode 3. It is probably due to the fact that the rotation of the robot arm is not fully captured by the representation of the second mode.

5. Conclusion

An experimental modal analysis was carried out in order to identify the joint stiffness and damping of a 6-axis industrial robot. Identified natural frequencies and damping ratios were used to update an elasto-dynamic model of the robot through a minimisation procedure. The robot was modelled using a multibody approach in which each link was connected by a torsional spring and a damper. Several comparisons were then conducted and revealed that the simulated robot reached the same natural frequencies with the same mode shapes. Although the comparison of the FRFs was not perfect, it is believed that the difference could come from a model limitation. Additional compliances should be added at the first three joints in order to capture their tilting oscillations around axes orthogonal to the motion axes.

Acknowledgment

The authors would like to acknowledge the Belgian National Fund for Scientific research (FNRS-FRS) for the FRIA grant allotted to H. N. Huynh.

REFERENCES

1. I. Iglesias, M.A. Sebastian, J.E. Ares. Overview of the state of robotic machining: Current situation and future potential, *Procedia Engineering*, **132**, 911–917, (2015).

2. O. Verlinden, H.N. Huynh, G. Kouroussis, E. Rivière-Lorphèvre. Modelling of flexible bodies with minimal coordinates by means of the co-rotational formulation, *Multibody System Dynamics*, pp. 1–20, (2017).

3. H.N. Huynh, E. Rivière-Lorphèvre, O. Verlinden. Integration of machining simulation within a multibody framework: application to milling, *In: Proceedings of the 4th Joint International Conference on Multibody System Dynamics IMSD*, (Canada, June, 2016).

4. Seifeddine Mejri, *Identification et modélisation du comportement dynamique des robots d'usinage (EN: Identification and modelling of milling robot dynamic behaviour)*, Ph.D. thesis, Blaise Pascal University - Clermont-Ferrand II, (2016).

5. H. Karagulle, A. Amindari, M. Akdag, L. Malgaca and S. Yavuz. Kinematic-Kinetic-Rigidity Evaluation of a Six Axis Robot Performing a Task, *International Journal of Advanced Robotic Systems (Mechatronics)*, pp. 1–9, (2012).

6. J. Bauer, M. Friedmann, T. Hemker, M. Pischan, C. Reinl, E. Abele and O. von Stryk, (2013), *Process Machine Interactions: Prediction and Manipulation of Interactions between Manufacturing Processes and Machine Tool Structures*, chap. 11 Analysis of Industrial Robot Structure and Milling Process Interaction for Path Manipulation, pp. 250–263. Springer.

7. M. Neubauer, H. Gattringer, A. Müller, A. Steinhauser and W. Höbarth. A two-stage calibration method for industrial robots with joint and drive flexibilities, *Mechanical Sciences*, **6**, (2015).

8. C. Dumas, S. Caro, S. Garnier and B. Furet. Joint stiffness identification of six-revolute industrial serial robots, *Robotics and Computer-Integrated Manufacturing*, **27**, 881–888, (2011).

9. N. M. M. Maia and J. M. M. Silva, *Theoretical and experimental modal analysis*, John Wiley & Sons (1997).

10. O. Verlinden, L. Ben Fékih and G. Kouroussis. Symbolic generation of the kinematics of multibody systems in EasyDyn: From MuPAD to Xcas/Giac, *Theoretical and Applied Mechanics Letters*, **3**, (2013).

11. G. Kouroussis, L. Ben Fekih, C. Conti and O. Verlinden. EasyMod: A MatLab/SciLab toolbox for teaching modal analysis, *Proceedings of the 19th International Congress on Sound and Vibration*, (2012).